Reciprocating-sliding wear behaviour of nanostructured and ultra-fine high-silicon bainitic steels

R. Rementeria[a], I. García[b], M.M. Aranda[a], F.G. Caballero[a]

[a]Department of Physical Metallurgy, Spanish National Center for Metallurgical Research (CENIM-CSIC), Avda. Gregorio del Amo 8, E-28040 Madrid, Spain, rosalia.rementeria@cenim.csic.es, m.m.aranda@cenim.csic.es, fgc@cenim.csic.es

[b]Department of Surface Engineering, Corrosion and Durability, Spanish National Centre for Metallurgical Research (CENIM-CSIC), Avda. Gregorio del Amo 8, E-28040 Madrid, Spain, igarcia@cenim.csic.es

Abstract

The reciprocating sliding wear behaviour of high-silicon bainitic steels has been studied on microstructures obtained from two alloys containing 0.3 and 1.0 wt.% C, which were isothermally transformed between 200 and 425 ºC. Results show an order of magnitude improvement in the wear resistance of the nano-scaled bainitic structures with respect to the ultra-fine with similar hardness values. The scale of the microstructure and the level of retained austenite determine the wear mechanism and eventually, the wear rate.

Keywords: Sliding wear; steel; microstructure; carbide-free bainite; nanostructured materials; hardness.

1. Introduction

The Nano Era has strongly flooded current research in materials engineering, and leading institutions and companies are hunting the benefits that the nano-scale provides. In steel industry, the term "ultra-fine" is generally used to describe materials with average grain sizes between 1 and 2 μm, and the term "submicron" (submicrometre) is used to refer to grain sizes between 100 and 1000 nm. The term "nanostructured" remains for those materials with a grain size lower than 100 nm.

Nanostructured bainite has been gaining considerable attention in recent years due to the extraordinary mechanical properties that can be achieved in a structure produced solely by isothermal holding after austenitization. Although quite a lot of work can be found in the literature devoted to the elementary mechanical properties of nanostructured bainite [1-5], there is still a long way to go before engineering the optimum nanostructures according the requirements for each in-use case, including wear resistance.

Earlier work on the potential of carbide-free bainite for wear applications [6-8] has been mainly focused on rails, showing excellent results on medium-carbon high-silicon steels under rolling-sliding wear conditions. The low wear rates achieved are attributed to the absence of carbides, the ability of the microstructures to tolerate a large degree of plastic strain and the mechanically induced martensitic transformation of retained austenite. The design of low-temperature

nanostructured bainitic steels would in principle result in exactly that direction of improvement, and they are therefore expected to lead to excellent wear resistance.

Former research on wear resistance of nanostructured bainite has been as well mainly focused in rolling-sliding wear [9-11], revealing that nanostructured steels exhibit significantly lower specific wear rates when compared to the reference 100Cr6 with lower bainite microstructure and other conventional carbide-free bainitic steels, even at the same hardness levels. Since hardness affects the stress needed to deform the material in the rolling/sliding contact, it is a paramount factor in decreasing material loss. Retained austenite provides hardening by transformation into martensite, so it is considered to be decisive for improving wear resistance. There have been a few timid forward steps among rolling contact fatigue [12, 13], dry sliding wear [14-16] and abrasive wear [17] of nanostructured bainite, with promising results.

The present work evaluates the reciprocating-sliding wear behaviour, not yet reported for high-silicon bainitic steels, in both ultra-fine carbide-free bainite and nanostructured bainite as compared to conventional pearlitic and quenched and tempered microstructures.

Reciprocating-sliding wear conditions selected for this work are similar to those withstood in opto-mechanical applications that require motion, such as focus adjustments and zooms. Here, wear resistance becomes important since it influences the stability and repeatability in the kinematic system [1]. The use of lubricants is normally restricted in these applications to avoid problems related to the migration of the lubricant and the subsequent contamination of the optical surfaces. Friction is therefore the most important contribution to wear in opto-mechanical systems. As a rough rule of thumb, friction coefficients and wear are minimized by using dissimilar materials in contact, as for example, alumina on steel.

2. Experimental

2.1 Material

The chemical compositions of the alloys investigated are 0.30C-1.48Si-2.06Mn-0.43Cr-0.27Mo, and 0.99C-2.47Si-0.74Mn-0.12Ni-0.97Cr-0.03Mo-0.17Cu wt. %, encoded as 0.3C and 1.0C, respectively.

Two steels with different carbon contents transforming to bainite in a wide range of temperatures were selected to achieve different bainitic structures with dissimilar amount, size and distribution of phases. The bainite transformation temperature range of the steel, delimited by the bainite start temperature (B_S) and the martensite start temperature (M_S), is mainly a consequence of the carbon content [18]. At the same time, the length-scale of the structures is directly related to the transformation temperature [19], the length-scale decreasing with decreasing the transformation temperature. By increasing the carbon content of the steel, there is allowance for lower transformation temperatures associated with finer microstructures.

Thus, 0.3C alloy, with a M_S of 300 ºC and a B_S of 450 ºC, was transformed after austenitization at 325, 350, 425 and 450 °C during 30 min in all the cases. Meanwhile 1.0C alloy, with a M_S of 170 ºC and a B_S of 350 ºC, was transformed after austenitization at 200, 250, 300 and 350 °C during 40, 15, 10 and 8 h, respectively. Austenitisation temperatures selected were 925 ºC for 0.3C steel and 950 ºC for 1.0C steel to ensure carbide dissolution during reheating of the as-received microstructure of the steels. Samples have been encoded as *x*C/*y*, where *x* is the carbon content of the alloy and *y* is the transformation temperature.

Heat treatments were performed in the furnace of an Adamel Lhomargy LK02 high resolution dilatometer on samples of 15 mm × 10 mm × 5 mm. Each sample was heated by radiation to the austenitization temperature for 15 min and subsequently cooled down to the isothermal temperature at a cooling rate of 50 ºC/s, the whole process being carried out in vacuum. Finally samples were helium quenched to room temperature.

In addition, other three conventional structures were produced from 1.0C heat, namely one pearlitic structure continuously cooled at 1.5 ºC/s, 1.0C/PER, and two samples tempered at 400 and 500 ºC after quenching, namely 1.0C/QT400 and 1.0C/QT500, respectively. This steel was selected to ensure a fully pearlitic structure after a slow cooling and a fully martensitic transformation after quenching. Further tempering on martensitic structures was performed to achieve hardness values comparable to that of bainitic structures.

2.2. Microstructural analysis

Samples for metallographic observation were ground, polished down to 1μm diamond paste and etched in 2% Nital solution. The unworn microstructures were examined by optical microscopy (OM), field emission gun-scanning electron microscopy (FEG-SEM). In the case of the nanostructured bainite samples (obtained in the 1.0C alloy), high magnification FEG-SEM micrographs were used to determine the bainitic ferrite plate thickness, *t*. If a plate is represented by a disk of radius *r* and thickness *t* with *r»t*, then the mean linear intercept length obtained by projecting random test lines is given by $\bar{L} = 2t$ [20]. However, in bainitic steels it is handier to measure the mean intercept, which is obtained by orienting the test line in the shortest direction of the plate, i.e. in a direction normal to the plate length. As derived in [21], the stereological correction used for the mean intercept method is $\overline{L_T} = \frac{\pi}{2}t$. The measurements provided are the average of at least 300 ferrite plates in several micrographs, and the error is merely given by the standard deviation of these measurements.

With regard to bainitic steels, additions of 1.5 wt.% silicon prevent the precipitation of cementite between the subunits of bainitic ferrite during bainitic transformation [22]. The carbon that is rejected from the bainitic ferrite enriches the surrounding austenite, so that it can be stabilised down to room temperature. The microstructure in high-silicon bainitic steels roughly consists of bainitic ferrite interwoven by retained austenite regions, though martensite regions might appear when the austenite carbon enrichment is insufficient.

Quantitative XRD analysis was employed to determine the fraction of retained austenite by the Rietveld refinement method, as described in [23]. For these experiments, samples were machined, ground and polished down to 1μm diamond paste, followed by several cycles of etching and polishing to remove surface deformation; finally the samples were polished in colloidal silica. X-ray diffraction measurements were performed with a Bruker AXS D8 diffractometer equipped with a Co X-ray tube and Goebel mirror at a current of 30 mA and a voltage of 40 keV.

In the case of the 1.0C steel, the level of carbon in the austenite after the transformation ensures that no martensite will be formed. Here, only two phases are present; the austenite (determined by XRD) and the bainitic ferrite, whose content is the balance.

Meanwhile, in the bainitic microstructures produced from 0.3C steel, it is likely that the carbon enrichment of large regions of austenite is not sufficient for the austenite to be stable at ambient temperature, so that martensite is expected to be formed during the last quenching stage after bainitic transformation. Martensite and ferrite peaks are not distinguishable in the XRD spectra, while martensite and austenite are neither distinguishable as individual phases, but identified as Martensite/Austenite (M/A) constituent by optical or scanning electron microscopy. For quantification of individual phases, FEG-SEM images are used to determine the M/A content following the Standard Test Method for Determining Volume Fraction by Systematic Manual Point Count (ASTM E562-11), which provides, after a suitable number of placements, an unbiased statistical estimate of the volume fraction of M/A. The martensite volume fraction is further obtained by subtracting from the M/A content the austenite content as determined by XRD. The bainitic ferrite amount would be the balance. The error bars are the addition of the systematic error of the XRD measurements (±3%) and the standard deviation of the Manual Point Count measurements, which varies for each case.

At last, to characterize the hardness of the bulk materials produced, macroscale vickers measurements were performed at a load of 30 kgf (HV30).

2.3. Wear tests

Room temperature dry sliding-wear tests were performed on the Bruker-UMT 2 tester in a reciprocating ball-on-plate configuration. Since the structures to be examined are dissimilar in scale, hardness and mechanical properties, the use of an inert material with a negligible wear coefficient against steel is necessary for sensible comparisons between them without any differential effect of the counterbody. For this reason, a non-metallic very hard counterbody is preferable in comparison with any specific steel. Therefore, alumina balls of 6 mm diameter were selected as counterbody over steel plates of 15 mm × 10 mm × 5 mm in polished condition (surface roughness, $R_a \sim 0.02\ \mu m$). All samples were ultrasonically cleaned with acetone and ethanol, and dried before and after each test.

A design method for minimizing wear for reciprocating sliding contacts is the engineering model for wear developed by Bayer (the zero wear model) [24, 25], where the maximum contact shear stress τ_{max} is given as a function of the number of cycles n and the shearing yield stress of the material τ_y by

$$\tau_{\max} \leq \left(\frac{2000}{n}\right)^{1/9} \gamma_R \tau_y \quad [24] \qquad \text{Eq. 1}$$

where γ_R is the zero wear coefficient, which is set equal to 0.54 in dissimilar materials. Typical values for the shearing yield stress in high-silicon bainitic steels range from 400 MPa in medium carbon alloys [26] up to 850 MPa in high carbon steels [3, 27]. Substituting in Eq. 1 the shearing yield stress value of 400 MPa representing the worst case and a number of 7200 cycles, the maximum contact stress allowed for a zero wear design is 187 MPa.

On the other hand, for the ball on plate geometry the maximum shearing stress occurring at the surface of the steel plate is given by

$$\tau_{\max} \approx q_0 \sqrt{\frac{1}{16}(1-2\nu)^2 + \mu^2} \qquad \text{Eq. 2}$$

where μ is the coefficient of friction (for steel/ceramics in sliding contact μ=0.5 [28]) , ν is the Poisson's ratio, and q_0 is the maximum pressure of the Hertzian initial point contact. Setting a contact load of 0.5 N, the maximum pressure of the elastic contact equals 360 MPa, and the maximum shearing stress obtained from Eq. 2 is 184 MPa. Therefore, the chosen experimental conditions should satisfy the zero wear model and in all cases the wear is expected to be mild.

Sliding velocities are relatively low in most opto-mechanical applications, whereas sliding distances vary for rough and accurate positioning depending on the system configuration and the manufacturer. A typical value of 5 mm for accurate motion regulation was selected as stroke length, at a frequency of 1 Hz, which leads to an average velocity of 10 mm/s.

Summarizing, tests were conducted with a contact load of 0.5 N, resulting in a maximum pressure of the Hertzian initial point contact of 360 MPa , running at 1 Hz with a reciprocating amplitude (stroke length) of 5 mm for 7200 cycles.

Four tests were carried out for each condition, and the wear loss was considered to be the average of the four tests. The volume of material loss for each wear track was computed from the length of the stroke and the average cross-sectional area, as measured by means of a laser confocal profilometer.

The volume wear loss of the plates was determined by means of an optical confocal profilometer, Sensofar PLμ2300, equipped with a high power LED blue light, operating in reflection mode with a Nikon 20XEPI objective and an emission wavelength of 460 nm. The wear volume loss was calculated from the average of the cross-sectional area measured at three locations centred in the wear track, and multiplied by the stroke length. The wear coefficient (k) was further obtained by dividing the volumetric wear loss by the total sliding distance and the contact load. The error bars correspond to the standard deviation of the wear coefficient of the four tests performed for each sample.

The worn surfaces were analyzed by FEG-SEM equipped with an energy dispersive X-ray spectroscopy (EDS) module, in order to qualitatively determine the presence of oxidation. In addition, bainitic samples were sectioned perpendicular to the worn surface and to the sliding direction in order to examine the microstructure of the deformed subsurface, as described in [29]. Cross-sections were examined by means of FEG-SEM for what the observation surfaces were tilted at 5º relative to normal incidence of the electron beam to precisely locate the microstructure below the wear tracks.

Finally, micro-hardness measurements were done centred over the wear track where the maximum reciprocating speed is achieved, using a load of 100 gf (HV0.1).

3. Results and discussion

3.1. Microstructure

Representative FEG-SEM micrographs of the microstructures obtained are shown in Figure 1. For 0.3C samples transformed at 325 and 350 ºC particles of cementite can be easily identified inside the ferrite plates, which are representative of lower bainite microstructures (Figure 1a). This steel transformed at higher temperatures, i.e. 425 and 450 ºC, leads to carbide-free bainitic ferrite laths with intervening M/A structures as seen in Figure 1b, embedded in a martensitic matrix. The volume fractions of phases shown in Figure 2 disclose that the amount of bainitic ferrite decreases with increasing the transformation temperature.

Microstructures obtained in the whole set of 1.0C steel transformed to bainite consist of bainitic ferrite plates interwoven by regions of films and blocks of austenite, as illustrated in Figure 1c and 1d. Measurements on the volume fraction of phases of the samples are collected in Figure 2a, where as it would be expected, the amount of bainitic ferrite decreases with increasing the transformation temperature.

At the same time, the scale of the bainitic microstructures obtained from 1.0C steel, in terms of bainitic ferrite plate thickness and austenite block size, is represented in Figure 2b. An example of the micrographs employed for the bainitic ferrite plate thickness determination is provided in Figure 3a. To ensure that the measurements are characteristic, typically two criteria are applied. First, the average of the measurements vs. the number of measurements must reach a plateau (see Figure 3c), what means that the data population is representative enough and the addition of extra data has no effect in the average value, though the standard deviation of the population would decrease. Second, the logarithmic-normal (lognormal) distribution of data is calculated and compared with the ideal log-normal distribution for the given mean and standard deviation. Nucleation and growth processes are usually described by the lognormal [30], so that a successful fitting ensures correct measurements, as in the example given in Figure 3b.

Here it can be seen that the scale of bainite increases with increasing the transformation temperature, from the nanoscale in 1.0C transformed at 200, 250 and 300 ºC to the sub-micron scale in 1.0C/350.

In general, bainitic structures hardness is inversely proportional to the amount of austenite, as seen in Figure 2a. When comparing both steels, further hardening is achieved in 1.0C structures by refining the bainitic ferrite plate thickness to the nanoscale.

Conventional microstructures obtained from 1.0C steel are shown in Figure 1e for the case of pearlite, and Figure 1f for the case of martensite tempered at 400 ºC. Bulk hardness values achieved in conventional microstructures are 409±4, 586±8 and 492±11 HV30 for 1.0C/PER, 1.0C/QT400 and 1.0C/QT500 respectively. It is noteworthy to mention that pearlitic microstructures obtained in a steel designed to produce low-temperature bainite, have an extremely-fine interlamellar spacing [31]. Under pure sliding and rolling-sliding conditions, fine interlamellar spacings have been demonstrated to decisively improve wear resistance [32, 33].

3.2 Wear

Wear resistance is determined by a combination of the hardness and toughness of materials. In the matter of sliding friction, hardness plays a greater role in wear resistance, owing to the small impact during sliding friction. In Figure 3 the specific wear rate (k) of the studied microstructures is plotted as a function of surface hardness after wear.

The wear rate vs. surface hardness after wear tendency for 0.3C bainitic steels is linear, in such a way that the lowest wear coefficient is attained by the sample with the hardest surface after wear. Nonetheless, a dependence on the transformation temperature nor the amount of phases is not observed. During the sliding contact the surface can be deformed and the hardness can change differently depending on the hardening ability of each material. For the studied steels, cold working and the transformation of retained austenite into martensite under strain (TRIP effect) are the key factors of the surface hardening. By comparing hardness values after and before wear of 0.3C samples in Figure 2a, the highest surface hardening and best wear performance was reached by the 0.3C/425. This latter microstructure, along with 0.3C/325 and

0.3C/350 show the same bulk hardness before testing and substantial differences in the volume fraction of the phases; while having similar amount of austenite, 0.3C/425 sample has a lower content in bainitic ferrite (see Figure 2a). In addition, the morphology of 0.3C/425 consists of carbide-free bainite, while the formers have a lower bainite microstructure. It is speculated that the higher initial dislocation density in lower bainite of medium-carbon high-silicon steels leads to a lower work-hardening rate [34], what would eventually come out in lower surface hardening and higher wear rate as compared to carbide-free bainite. Therefore, it can be stated that for this steel the dry reciprocating-sliding wear performance of carbide-free bainitic microstructures is better than that of the lower bainite.

Contrastingly, the wear coefficient of 1.0C bainitic steels shows independence of hardness after wear, and it is comparable to that of the reference steels, while also being twice lower than the best of the 0.3C microstructures. The lack of correlation of hardness with wear resistance had previously been observed on dry-sliding wear of carbide-free bainitic steels elsewhere [35-37], so that wear resistance of these bainitic steels depends critically on the microstructure of the sample and thus on the transformation conditions. From the comparisons among 1.0C bainitic steels, it is observed that higher hardening rates are achieved by lowering the transformation temperature, unlike what was observed in 0.3C bainitic steels. In nanostructured bainitic structures the transformation induced plasticity of the austenite implies strain hardening by means of the progressive increase in the volume fraction of martensite and additional plastic deformation due to transformation strains. Interestingly, the highest hardening rate is achieved in the 1.0C sample transformed at 200 ºC, whose amount of austenite is the lowest, querying whether the hardness increase achieved in 1.0C steel is the result of retained austenite decomposition within the surface, or consequence of a more conventional form of cold-working.

3.4. Worn surface observations

The different wear behaviour found for 0.3C and 1.0C bainitic steels can be related to the diverse wear mechanisms acting during testing. Figure 4 shows FEG-SEM micrographs of the wear tracks on the studied microstructures.

Regarding the wear process, the chemical affinity between the alumina ball and the steel is negligible, so the interaction between the mating surfaces is principally due to mechanical effects. Even so, the test configuration involves the presence of wear debris between sliding surfaces, which could be beneficial by reducing adhesion or by acting in the manner of a roller bearing, thereby reducing the wear rate, or could be detrimental by leading to abrasive wear.

Wear mechanism in 0.3C microstructures does not vary among them, and is exemplified in Figure 4a. The main damage micromechanisms observed are grooves running in the sliding direction and plastically deformed side ridges around the grooves, indicating that abrasive wear is mainly taking place. There are also observed indentations and accumulation of irregular oxidized wear debris at the indentations, as illustrated in Figure 4d. These indentations can be either the result of flakes of material that were abraded from the surface, or debris that have oxidized and accumulated in the surface that are hard enough to cause indentation damage when pressed into the tribological contact [7]. As the same wear mechanism is acting in all 0.3C samples, the degree of wear will be hardness-dependent [38], as seen in Figure 3.

In 1.0C/200 and 1.C/250, the worn surface is almost not oxidized and grooves from abrasion are also observed, though in this case prominent ridges are not present, as depicted in Figure 4b. In

1.0C/300 and 1.0C/350 (see Figure 4c) slight abrasion is also observed combined with the presence of shear tongues caused by plastic deformation in the contact region under compression and shearing, which would result in crack initiation and propagation in the combined fracture mode of tensile and shear in the trailing region of the contact [39]. The presence of shear tongues in 1.0C bainitic samples is illustrated in Figure 4e for 1.0C/200 and Figure 4f for 1.0C/350. Shear tongues, or delamination flakes in the samples transformed at lower temperature are somewhat tighter and cutting grooves from abrasion are evident in between them.

Transitions between abrasive micromechanisms, depend on the shearing strength at the mating interface, which is a function of the volume fraction and size of phases [38]. The described wear mechanisms in 1.0C bainitic samples change gradually from abrasion by microcutting to abrasion with a large degree of plastic deformation with increasing the transformation temperature. It is speculated that shear ductility provided by the austenite plays an important role in such a way that any particular volume of material remains longer at the surface before becoming a loose particle. Therefore, the wear process in 1.0C/200 and 1.0C/250, with a matrix consisting of slender plates of bainitic ferrite, would lead to very fine and hard debris that act by microcutting abrading out the wear scar bed. For 1.0C/300 and 1.0C/350, the high amount of the ductile phase (austenite) withstands larger plastic deformation, with less production of abrasive debris resulting in a wear rate comparable to that of the 1.0C transformed at lower temperatures.

Concerning the wear mechanisms in the conventional microstructures, Figure 4g and 4e illustrate the wear scar bed surfaces observed for the 1.0C pearlitic and 1.0C quenched and tempered steels. In 1.0C/PER the worn surface is comparable to that of 1.0C/350, but with a larger degree of plastic deformation and oxidation. As regards the quenched and tempered microstructures, a high amount of adhered particles stands out over the wear surface. Extensive oxidation of the worn surface was detected qualitatively by EDS. Figure 6a illustrates the spectra obtained for 1.0C/QT500, where the presence of a high oxygen peak in the wear track is noteworthy when compared to the spectrum obtained at the unworn surface. Oxidation at these surfaces without the removal of the oxides, justifies the low wear rates encountered.

The presence of oxides in the bainitic samples was seldom, if ever, little oxidation was detected at the side ridges of the wear track or at the adhered particles out of the track, as given in the examples of Figure 6b and 6c for 0.3C/425 and 1.0C/300 respectively.

Figure 7 illustrates the microstructure below the wear track on cross-sections of the specimens. In 0.3C bainitic samples, no substantial subsurface deformation nor the presence of a tribo-layer were observed, as exemplified in Figure 7a for 0.3C/325. In the case of 1.0C bainitic structures, the microstructural patterns across the wear tracks are not homogeneous: there are localized regions where the microstructure undergoes deformation and slightly alginates sideways below a groove, whereas other regions show neither deformation nor the presence of a tribo-layer. An example of these trends is given in Figure 7b for 1.0C/300, where the magnified micrograph on the right shows deformation of the microstructure close to the surface, while the magnified micrograph on the left shows no microstructural changes at the subsurface. As the behaviour of the microstructure is not uniform below the wear track, conclusions extracted from these observations must be handled with care. However, deformation of the microstructure in 1.0C bainitic steels (independently of its extent) should provide strengthening along with more resistance to material removal as compared to 0.3C bainitic steels.

4. Conclusions

Dry reciprocating-sliding wear tests have been conducted at low frequencies using the zero wear model on high-silicon bainitic and conventional steel plates against an alumina ball. Under these conditions, the wear resistance of high-carbon high-silicon bainitic steels is at least twice superior to that of medium-carbon high-silicon bainitic steels with similar hardness values.

The wear resistance of medium-carbon high-silicon bainitic steels depends linearly on surface hardness after wear, being better for the carbide-free bainite morphologies.

The independence of wear resistance to hardness in the case of the high-carbon high-silicon steel is due to the different micromechanisms of surface damage operating in each case, which in turn are microstructure-dependent. The highly refined microstructure and the transformation under strain of the austenite films, contributes to the surface hardening as to plastic deformation improving the wear performance.

Acknowledgements

The authors gratefully acknowledge the support of Ministerio de Economia y Competitividad (MINECO) and Fondo Europeo de Desarrollo Regional (FEDER) for funding this research under the Contract IPT-2012-0320-420000, as well the financial backing from the the Research Fund for Coal and Steel in the form of RFSR-CT-2014-00016.

References

[1] C. Garcia-Mateo, F.G. Caballero, H.K.D.H. Bhadeshia, Mechanical properties of low-temperature bainite, Microalloying for New Steel Processes and Applications, Trans Tech Publications Ltd, Zurich-Uetikon, 2005, pp. 495-501.

[2] C. Garcia-Mateo, F.G. Caballero, The role of retained austenite on tensile properties of steels with bainitic microstructures, Mater. Trans. JIM, 46 (2005) 1839-1846.

[3] F.G. Caballero, H.K.D.H. Bhadeshia, Very strong bainite, Curr. Opin. Solid State Mat. Sci., 8 (2004) 251-257.

[4] H.K.D.H. Bhadeshia, Properties of fine-grained steels generated by displacive transformation, Mater. Sci. Eng. A, 481-482 (2008) 36-39.

[5] M. Soliman, H. Palkowski, Ultra-fine bainite structure in hypo-eutectoid steels, ISIJ Int., 47 (2007) 1703-1710.

[6] L.C. Chang, The rolling/sliding wear performance of high silicon carbide-free bainitic steels, Wear, 258 (2005) 730-743.

[7] A. Leiro, A. Kankanala, E. Vuorinen, B. Prakash, Tribological behaviour of carbide-free bainitic steel under dry rolling/sliding conditions, Wear, 273 (2011) 2-8.

[8] E. Vuorinen, L. Wan, S. Stanojevic, B. Prakash, Influence of retained austenite on rolling-sliding wear resistance of austempered silicon alloyed steel, Proceedings of Hot Sheet Metal Forming of High-Performance Steel, 2nd International Conference, (2009).

[9] A. Leiro, E. Vuorinen, K.G. Sundin, B. Prakash, T. Sourmail, V. Smanio, F.G. Caballero, C. Garcia-Mateo, R. Elvira, Wear of nano-structured carbide-free bainitic steels under dry rolling–sliding conditions, Wear, 298–299 (2013) 42-47.

[10] T. Sourmail, F.G. Caballero, C. Garcia-Mateo, V. Smanio, C. Ziegler, M. Kuntz, R. Elvira, A. Leiro, E. Vuorinen, T. Teeri, Evaluation of potential of high Si high C steel nanostructured bainite for wear and fatigue applications, Mater. Sci. Technol., 29 (2013) 1166-1173.

[11] S. Das Bakshi, A. Leiro, B. Prakash, H.K.D.H. Bhadeshia, Dry rolling/sliding wear of nanostructured bainite, Wear, 316 (2014) 70-78.

[12] H. Liu, J. Sun, T. Jiang, S. Guo, Y. Liu, Improved rolling contact fatigue life for an ultrahigh-carbon steel with nanobainitic microstructure, Scr. Mater., 90–91 (2014) 17-20.

[13] W. Solano-Alvarez, E.J. Pickering, H.K.D.H. Bhadeshia, Degradation of nanostructured bainitic steel under rolling contact fatigue, Mater. Sci. Eng. A, 617 (2014) 156-164.

[14] T.S. Wang, J. Yang, C.J. Shang, X.Y. Li, B. Lv, M. Zhang, F.C. Zhang, Sliding friction surface microstructure and wear resistance of 9SiCr steel with low-temperature austempering treatment, Surf. Coat. Technol., 202 (2008) 4036-4040.

[15] P. Zhang, F.C. Zhang, Z.G. Yan, T.S. Wang, L.H. Qian, Wear property of low-temperature bainite in the surface layer of a carburized low carbon steel, Wear, 271 (2011) 697-704.

[16] J. Yang, T.S. Wang, B. Zhang, F.C. Zhang, Sliding wear resistance and worn surface microstructure of nanostructured bainitic steel, Wear, 282–283 (2012) 81-84.

[17] S. Das Bakshi, P.H. Shipway, H.K.D.H. Bhadeshia, Three-body abrasive wear of fine pearlite, nanostructured bainite and martensite, Wear, 308 (2013) 46-53.

[18] C. Garcia-Mateo, T. Sourmail, F. Caballero, C. Capdevila, C. de Andres, New approach for the bainite start temperature calculation in steels, Mater. Sci. Technol., 21 (2005) 934-940.

[19] S.B. Singh, H.K.D.H. Bhadeshia, Estimation of bainite plate-thickness in low-alloy steels, Mater. Sci. Eng. A, 245 (1998) 72-79.

[20] E.E. Underwood, Quantitative stereology, Addison-Wesley Pub. Co., 1970.

[21] L.C. Chang, H.K.D.H. Bhadeshia, Austenite Films In Bainitic Microstructures, Mater. Sci. Technol., 11 (1995) 874-881.

[22] E. Kozeschnik, H.K.D.H. Bhadeshia, Influence of silicon on cementite precipitation in steels, Mater. Sci. Technol., 24 (2008) 343-347.

[23] C. Garcia-Mateo, F.G. Caballero, M.K. Miller, J.A. Jimenez, On measurement of carbon content in retained austenite in a nanostructured bainitic steel, J. Mater. Sci., 47 (2012) 1004-1010.

[24] J.H. Dumbleton, S.H. Rhee, The application of a zero wear model to metal/ polyethylene sliding pairs, Wear, 35 (1975) 233-250.

[25] R.G. Bayer, W.C. Clinton, C.W. Nelson, R.A. Schumacher, Engineering model for wear, Wear, 5 (1962) 378-391.

[26] F.G. Caballero, S. Allain, J. Cornide, J.D. Puerta Velásquez, C. Garcia-Mateo, M.K. Miller, Design of cold rolled and continuous annealed carbide-free bainitic steels for automotive application, Mater. Des., 49 (2013) 667-680.

[27] C. Garcia-Mateo, F.G. Caballero, T. Sourmail, M. Kuntz, J. Cornide, V. Smanio, R. Elvira, Tensile behaviour of a nanocrystalline bainitic steel containing 3 wt% silicon, Mater. Sci. Eng. A, 549 (2012) 185-192.

[28] A. Gangopadhyay, S. Jahanmir, M.B. Peterson, Self-lubricating ceramic matrix composites, Friction and Wear of Ceramics, (1994) 163-197.

[29] S. Sharma, S. Sangal, K. Mondal, Influence of Subsurface Structure on the Linear Reciprocating Sliding Wear Behavior of Steels with Different Microstructures, Metall. Mater. Trans. A, 45 (2014) 6088-6102.

[30] R.B. Bergmann, A. Bill, On the origin of logarithmic-normal distributions: An analytical derivation, and its application to nucleation and growth processes, J. Cryst. Growth, 310 (2008) 3135-3138.

[31] K.M. Wu, H.K.D.H. Bhadeshia, Extremely fine pearlite by continuous cooling transformation, Scr. Mater., 67 (2012) 53-56.

[32] A.J. Perez-Unzueta, J.H. Beynon, Microstructure and wear resistance of pearlitic rail steels, Wear, 162–164, Part A (1993) 173-182.

[33] P. Clayton, D. Danks, Effect of interlamellar spacing on the wear resistance of eutectoid steels under rolling-sliding conditions, Wear, 135 (1990) 369-389.

[34] X.Y. Long, F.C. Zhang, J. Kang, B. Lv, X.B. Shi, Low-temperature bainite in low-carbon steel, Mater. Sci. Eng. A, 594 (2014) 344-351.

[35] P. Clayton, K.J. Sawley, P.J. Bolton, G.M. Pell, Wear behavior of bainitic steels, Wear, 120 (1987) 199-220.

[36] P.H. Shipway, S.J. Wood, A.H. Dent, The hardness and sliding wear behaviour of a bainitic steel, Wear, 203–204 (1997) 196-205.

[37] Y. Wang, T. Lei, Wear behavior of steel 1080 with different microstructures during dry sliding, Wear, 194 (1996) 44-53.

[38] K. Hokkirigawa, K. Kato, Z.Z. Li, The effect of hardness on the transition of the abrasive wear mechanism of steels, Wear, 123 (1988) 241-251.

[39] B. Bhushan, M. Nosonovsky, Scale effects in friction using strain gradient plasticity and dislocation-assisted sliding (microslip), Acta Mater., 51 (2003) 4331-4345.

Figure captions

Figure 1. FEG-SEM micrographs of the unworn microstructures for: a) 0.3C/325, b) 0.3C/450, c) 1.0C/200, d) 1.0C/350, e) 1.0C/PER and f) 1.0C/QT400.

Figure 2. Quantitative data on the unworn bainitic microstructures: a) Volume fraction of constituent phases and surface hardness before wear (HV30), and after wear (HV0.1), and b) Bainitic ferrite plate thickness and austenite block size for 1.0C bainitic samples.

Figure 3. a) High magnification FEG-SEM micrograph of 1.0C/300 structure employed for bainitic ferrite plate thickness measurements, b) bainitic ferrite plate thickness distribution of 1.0C/300 structure (bars) and corresponding log-normal distribution (dashed line) for the average and standard deviation of the values measured, and c) Average bainitic ferrite plate thickness as a function of the number of measurements in 1.0C bainitic steels.

Figure 4. Specific wear rate vs. surface hardness after wear of the studied samples.

Figure 5. FEG-SEM micrographs showing the surface morphology of the wear scar bed of the bainitic structures exemplified for a) 0.3C/350, b) 1.0C/200, c)1.0C/350, and corresponding magnified micrographs for d) 0.3C/350, e) 1.0C/200 and f)1.0C/350. Surface morphology of the wear scar bed of the conventional structures exemplified for g)1.0C/PER and h)1.0C/QT500. The double arrow in a) indicates the sliding direction.

Figure 6. FEG-SEM micrographs of the wear scar bed and corresponding EDS spectra of the indicated areas of a) 1.0C/QT500, b) 0.3C/425 and c) 1.0C/300. The double arrow in a) indicates the sliding direction.

Figure 7. FEG-SEM micrographs below the wear track on cross-sections tilted 5º relative to normal incidence of the electron beam for a) 0.3C/325 and b) 1.0C/300. Magnified micrographs correspond to the squared areas, and the double arrow indicates the sliding direction over the wear surface.

Figure 1

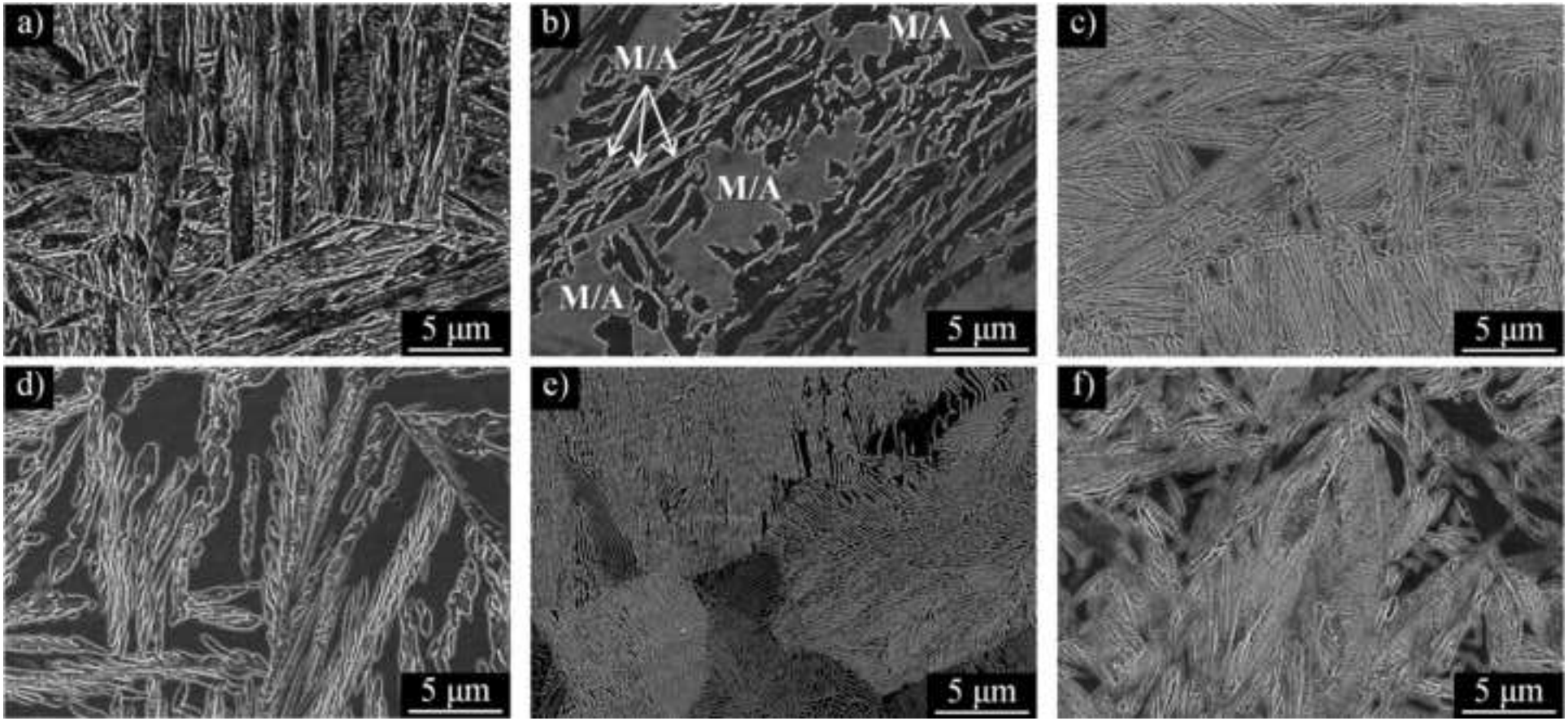

Figure 2

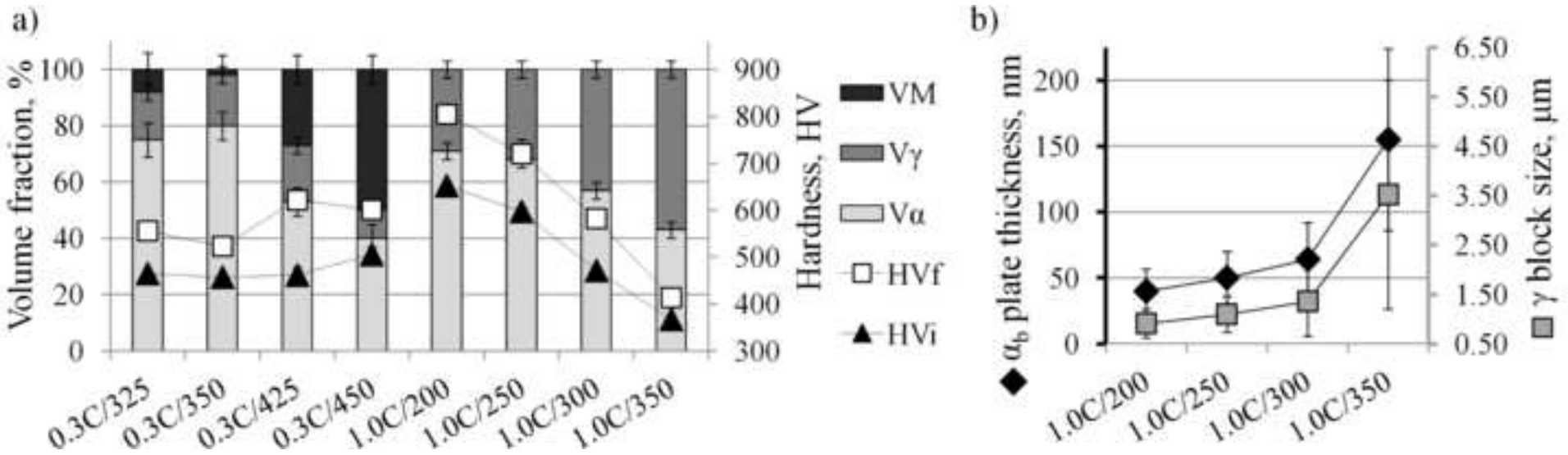
a)
Volume fraction, %
100
80
60
40
20
0
900
800
700
600
500
400
300
Hardness, HV
VM
Vγ
Vα
HVf
HVi
0.3C/325
0.3C/350
0.3C/425
0.3C/450
1.0C/200
1.0C/250
1.0C/300
1.0C/350
b)
α_b plate thickness, nm
200
150
100
50
0
6.50
5.50
4.50
3.50
2.50
1.50
0.50
γ block size, μm
1.0C/200
1.0C/250
1.0C/300
1.0C/350

Figure 3

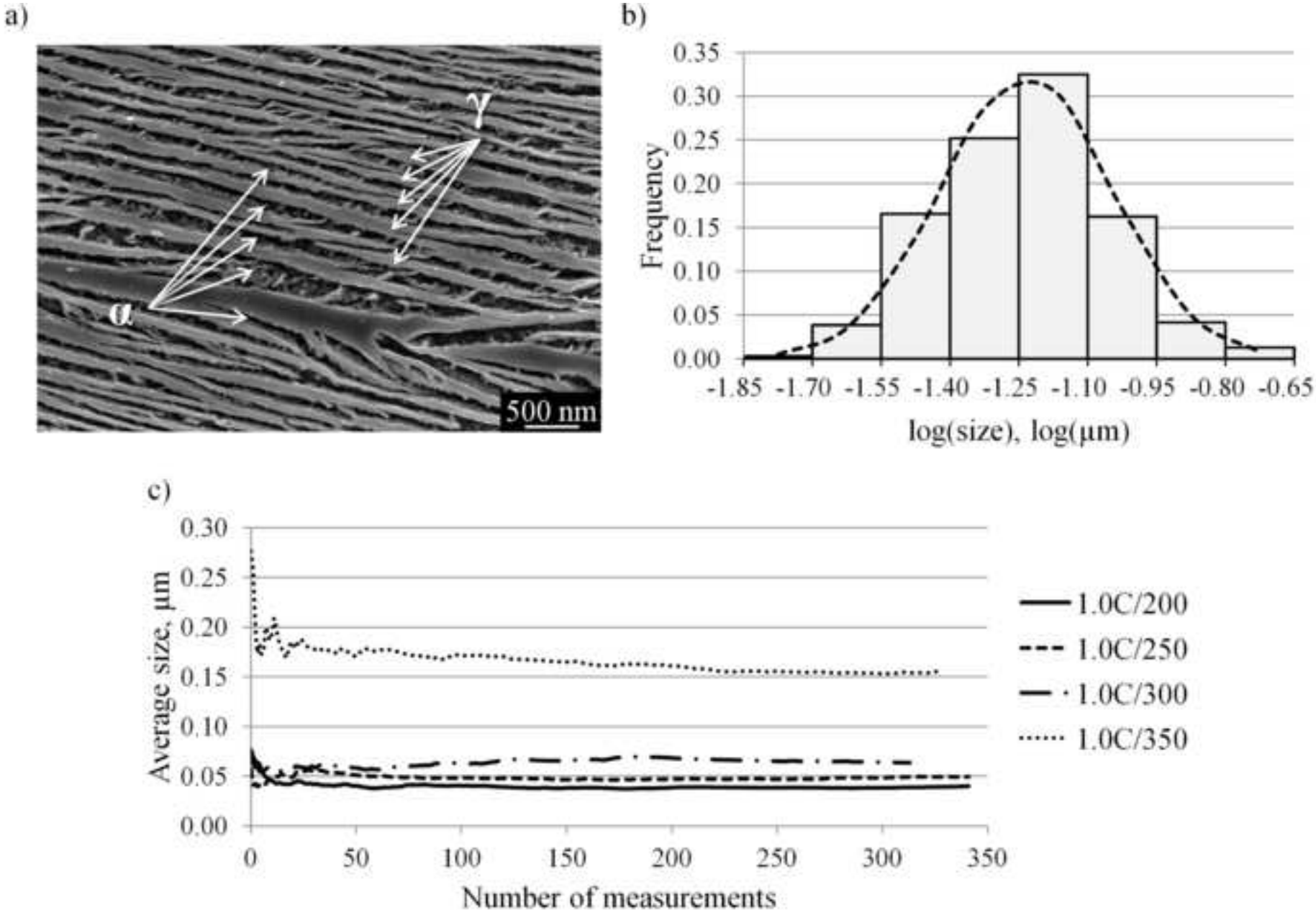
a)
γ
α
500 nm
b)
Frequency
0.35
0.30
0.25
0.20
0.15
0.10
0.05
0.00
-1.85 -1.70 -1.55 -1.40 -1.25 -1.10 -0.95 -0.80 -0.65
log(size), log(μm)
c)
Average size, μm
0.30
0.25
0.20
0.15
0.10
0.05
0.00
0 50 100 150 200 250 300 350
Number of measurements
1.0C/200
1.0C/250
1.0C/300
1.0C/350

Figure 4

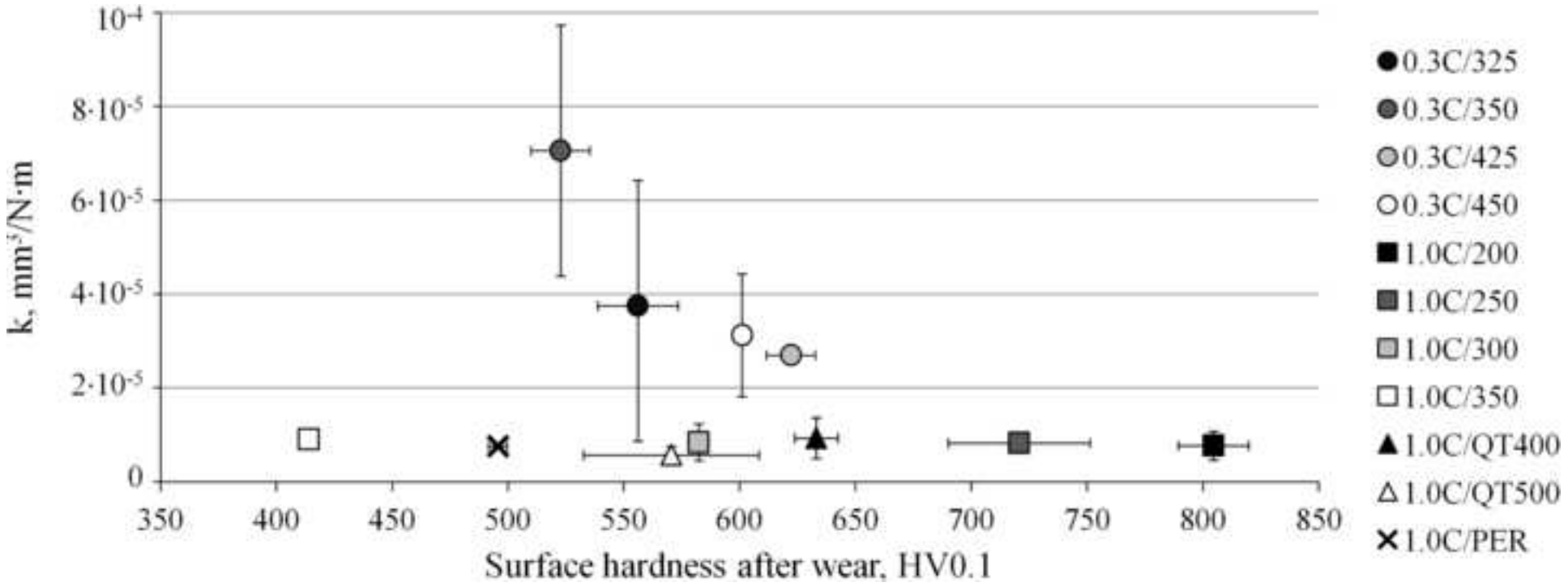
k, mm³/N·m
10⁻⁴
8·10⁻⁵
6·10⁻⁵
4·10⁻⁵
2·10⁻⁵
0
350
400
450
500
550
600
650
700
750
800
850
Surface hardness after wear, HV0.1
0.3C/325
0.3C/350
0.3C/425
0.3C/450
1.0C/200
1.0C/250
1.0C/300
1.0C/350
1.0C/QT400
1.0C/QT500
1.0C/PER

Figure 5

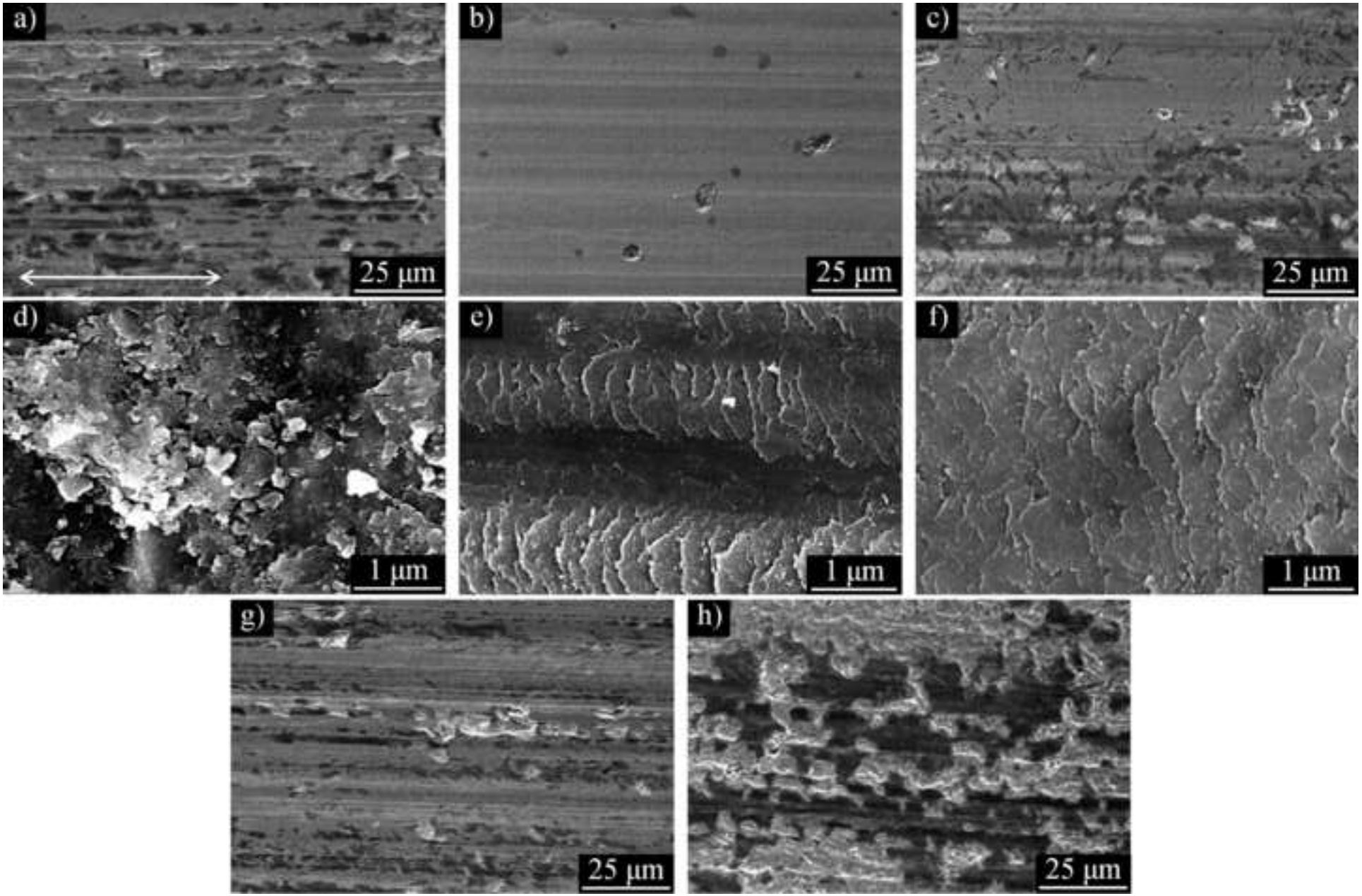

Figure 6

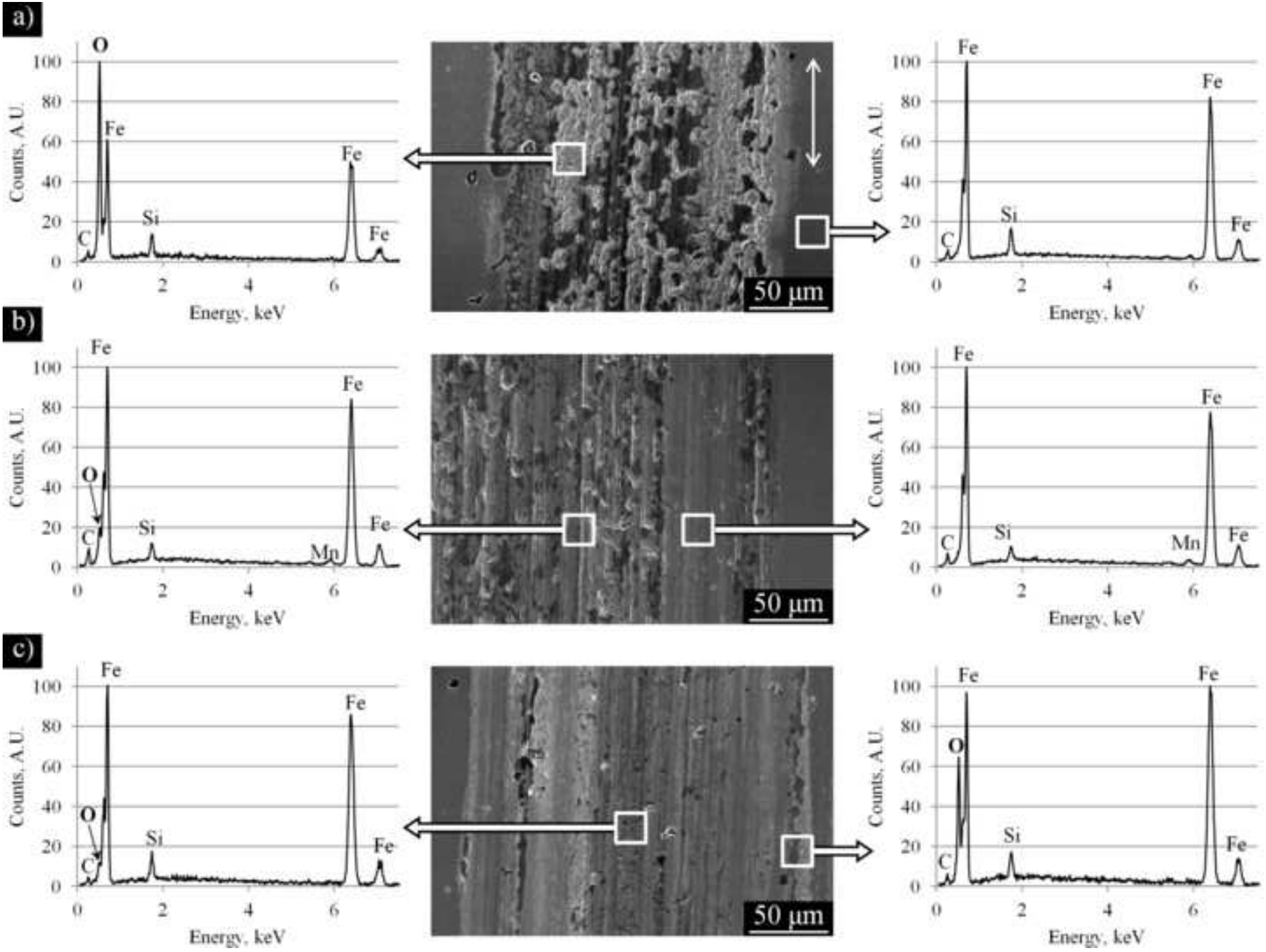

Figure 7